The microtubule plus-end tracking protein Bik1 is required for chromosome congression

Alexander Julner [1], Marjan Abbasi [1], and Victoria Menéndez-Benito [1,2]

[1] Department of Biosciences and Nutrition, Karolinska Institutet, SE-141 83, Huddinge, Sweden.

[2] Correspondence: victoria.menendez.benito@ki.se

Abstract

During mitosis, sister chromatids congress on either side of the spindle equator to facilitate the correct partitioning of the genomic material. Chromosome congression requires a finely tuned control of microtubule dynamics by the kinesin motor proteins. In *Saccharomyces cerevisiae*, the kinesin proteins Cin8, Kip1, and Kip3 have pivotal roles in chromosome congression. It has been hypothesized that additional proteins that modulate microtubule dynamics are also involved. Here, we show that the microtubule plus-end tracking protein Bik1 - the budding yeast ortholog of CLIP-170 – is essential for chromosome congression. We find that nuclear Bik1 localizes to the kinetochores in a cell-cycle-dependent manner. Disrupting the nuclear pool of Bik1 with a nuclear export signal (Bik1-NES) leads to a slower cell cycle progression characterized by a delayed metaphase-anaphase transition. Bik1-NES cells have mispositioned kinetochores along the spindle in metaphase. Furthermore, using proximity-dependent methods, we identify Cin8 as an interaction partner of Bik1. Deleting CIN8 reduces the amount of Bik1 at the spindle. In contrast, Cin8 retains its typical bilobed distribution in Bik1-NES and does not localize to the unclustered kinetochores characteristic of Bik1-NES cells. Thus, we propose that Bik1 functions together with Cin8 to regulate kinetochore-microtubule dynamics for correct kinetochore positioning and chromosome congression.

Keywords: mitosis, kinetochore, chromosome, kinesins, genetic stability.

Introduction

Cell division relies on the accurate segregation of sister chromatids to generate functional daughter cells. Before segregation, sister chromatids are positioned at the spindle equator through a process known as chromosome congression that culminates with the metaphase plate formation in metazoans (reviewed in (Maiato et al., 2017)). The establishment of a metaphase plate forces all the chromosomes to segregate from the same starting position, thereby contributing to faithful segregation. Despite the relevance of chromosome congression, its molecular mechanisms remain unclear.

The budding yeast *Saccharomyces cerevisiae* is an appealing model organism to study spindle dynamics because it is amenable to genetic engineering and has a relatively simple spindle. Budding yeast has 16 chromosomes. After duplication, each sister chromatid is linked by a kinetochore to a single kinetochore microtubule emanating from the spindle pole body (SPB), the yeast centrosome (Winey & O'Toole, 2001). Each SPB also gives rise to four interpolar microtubules, with plus-ends that overlap at the middle of the spindle (O'Toole et al., 1999; Peterson & Ris, 1976; Winey et al., 1995). In prometaphase, kinetochores congress in two opposite clusters near the spindle equator, equidistant from the SPBs. As in metazoan cells, this appears to occur prior to biorientation of sister chromatids (Marco et al., 2013).

Several studies have shown that kinetochore microtubules are regulated in a length-dependent manner (Gardner et al., 2005; Pearson et al., 2006; Sprague et al., 2003). Short microtubules tend to grow, whereas long microtubules that extend towards the spindle equator are destabilized and depolymerize. As sister chromatids are held together by cohesin, depolymerization of kinetochore

50 microtubules generates tension, mediated by the Ndc80 and Dam1 complexes' ability to track the
51 dynamic tips of the kinetochore microtubules (Powers *et al.*, 2009; Suzuki *et al.*, 2016).
52
53 Kinesin motors – proteins that move along microtubules powered by the hydrolysis of adenosine
54 triphosphate (ATP) – are involved in chromosome congression in several organisms (see Maiato *et*
55 *al.*, 2017, Table 1). In budding yeast, the deletion of the kinesins Cin8, Kip3, and, to a lesser extent,
56 Kip1, results in declustering of kinetochores (Gardner et al., 2008; Marco et al., 2013; Tytell & Sorger,
57 2006; Wargacki et al., 2010). Cin8 and Kip3 have been shown to act as length-dependent microtubule
58 depolymerases, promoting catastrophe of long microtubules (Gardner et al., 2008; Su et al., 2011;
59 Varga et al., 2006).
60
61 It has long been speculated that other microtubule-associated proteins could play a role in
62 chromosome congression (Kops *et al.*, 2010). Specifically, microtubule plus-end tracking proteins
63 (+TIPs) are interesting candidates, because they accumulate at kinetochore microtubule plus-ends
64 and regulate their dynamics (reviewed in Akhmanova & Steinmetz, 2010). Bik1, the yeast ortholog of
65 CLIP-170, is a +TIP protein that exists in cytoplasmic and nuclear pools within the cell (Carvalho et al.,
66 2004). The cytoplasmic pool is important for mitotic spindle positioning through both the Kar9 and
67 the dynein pathways (reviewed in Miller *et al.*, 2006). First, Bik1 promotes phosphorylation of Kar9
68 for asymmetric localization at the old SPB (Moore et al., 2006). Kar9, together with the +TIP protein
69 Bim1 and the actin-guided myosin motor protein Myo2, mediates the capture of astral microtubules
70 at the bud cortex, contributing to spindle alignment and nuclear migration (Xiang, 2018). During
71 anaphase, Bik1 is transported by the kinesin Kip2 to the plus-ends of astral microtubules, where it
72 facilitates the recruitment of dynein (Carvalho *et al.*, 2004; Roberts *et al.*, 2014). Dynein is a minus
73 end-directed motor and will exert a pulling force on the spindle that results in nuclear migration to
74 the bud.

75 The nuclear pool of Bik1 is associated with the spindle at SPBs and kinetochores (Carvalho et al.,
76 2004; Lin et al., 2001) but its function is not well understood. Early studies found that deleting BIK1
77 results in cells with short or non-detectable astral microtubules (Berlin *et al.*, 1990). In contrast, cells
78 overexpressing Bik1 display short spindle microtubules and long astral microtubules. In this study,
79 we investigate the nuclear function of Bik1 and its role in chromosome congression and cell cycle
80 progression.
81

82 # Results

83 ### Bik1 localizes to kinetochores in a cell cycle-dependent manner

84 We examined the localization of Bik1 in relation to tubulin, kinetochores and SPBs at different cell
85 cycle phases. We used cells expressing Bik1-superfolder GFP (sfGFP), mTurquoise-Tub1 (alpha
86 tubulin, microtubule marker), and either Ndc80-tagRFPT (kinetochore marker) or Spc42-tagRFPT (SPB
87 marker) (Figure 1A). In metaphase cells, nuclear Bik1 was primarily found between SPBs and
88 overlapping with kinetochores (Figure 1A, upper panels). By contrast, in anaphase cells, nuclear Bik1
89 was concentrated in patches along interpolar microtubules, while cytoplasmic Bik1 localized to astral
90 microtubules (Figure 1A, lower panels).
91

92 To confirm the metaphase association with kinetochores, we used cells expressing the APC/C co-
93 activator Cdc20 under control of the galactose inducible *GAL1* promoter. Shifting the carbon source
94 from galactose to glucose represses the expression of CDC20 and thereby arrests the cells at the
95 metaphase-to-anaphase transition. Bik1-sfGFP was also localized at kinetochore clusters in
96 metaphase-arrested cells (Figure 1B, upper panel), confirming what we observed in cycling cells. We
97 measured the distribution of Bik1-sfGFP in metaphase arrested cells and found that it had a bilobed
98 localization pattern like that of the kinetochore marker Ndc80-tagRFPT (Figure 1B, lower panel).
99

100 Nuclear Bik1 is needed for timely cell cycle progression

101 Bik1 in the cytoplasm localizes to astral microtubules and plays an important role in mitotic spindle
102 positioning (reviewed in Miller et al., 2006). To disrupt the kinetochore function of Bik1 while
103 maintaining its cytoplasmic function, we fused a strong nuclear export consensus sequence (NES)
104 (Kosugi et al., 2008) to the C-terminal end of Bik1-sfGFP or Bik1-5xFlag (collectively referred to as
105 Bik1-NES, Figure 1C). We imaged Bik1-NES cells expressing mTurquoise-Tub1, and Nc80-tagRFPT and
106 found that the mutant indeed excludes Bik1 from the nucleus (Figure 1D). To quantify the
107 effectiveness of the NES, we followed the localization of Bik1 in Bik1-sfGFP and Bik1-sfGFP-NES cells
108 expressing mTurquoise-Tub1. We synchronized the cells in G1 with α-factor, released them in fresh
109 media and imaged them at metaphase. As expected, Bik1-NES cells have significantly less sfGFP
110 signal at the spindle than Bik1 cells (Figure 1E-F).

111

112 We next assessed cell cycle progression in the absence of nuclear Bik1. We synchronized Bik1-sfGFP
113 and Bik1-sfGFP-NES cells in G1 with α-factor. Then, we released the cells from the G1 block and
114 prepared fixed samples at 10 min intervals. We scored the number of cells in G1/S, metaphase, or
115 anaphase according to the spindle length (mRuby2-Tub1) (Figure 2A). The strain expressing Bik1-
116 sfGFP had a sharp peak of metaphase cells at 40 min and a high number of cells with long spindles
117 50-60 min after the release. Bik1-sfGFP-NES cells, by contrast, displayed a broader peak of
118 metaphase cells that spans between 40-60 min post-release, and a 10 min delay in the anaphase
119 peak.

120

121 We then examined Bik1-sfGFP and Bik1-sfGFP-NES cells after G1 synchronization with α-factor by
122 time-lapse imaging (Figure 2B-E). In the Bik1-sfGFP strain, Bik1 was localized to the kinetochores
123 from G1 through metaphase. When the spindle elongates in anaphase, Bik1 was no longer associated
124 with the kinetochores and was found in patches along the interpolar microtubules instead (Figure
125 2B-C), as observed in fixed cells. The fluorescence intensity of Bik1-sfGFP at kinetochores was

126 greatest at metaphase when kinetochores cluster and reduced to near background levels in
127 anaphase (Figure 2D). In agreement with the analysis from fixed cells, we observed a slight delay in
128 cell cycle progression in Bik1-NES cells (Figure 2B, arrows). Our quantifications showed that the time
129 from the appearance of two kinetochore clusters to their segregation into mother and daughter cells
130 is approximately 10 min longer in Bik1-NES cells (Figure 2E).
131

132 ### Cells lacking nuclear Bik1 display aberrant kinetochore positioning

133 Because Bik1 localizes near the kinetochores in metaphase, we hypothesized that the prolonged
134 metaphase of Bik1-NES cells might be due to a dysregulation in kinetochore clustering. To test this
135 hypothesis, we analyzed the distribution of the kinetochore component Ndc80-sfGFP relative to the
136 SPBs (Spc42-tagRFPT) in cells expressing either Bik1-5xFlag or Bik1-5xFlag-NES arrested in metaphase
137 (PGal1-Cdc20) (Figure 3). While Bik1-5xFlag cells showed typical Ndc80 clusters, we observed cells
138 with long stretches of Ndc80 in the Bik1-5xFlag-NES mutant (Figures 3A-B). The unclustered
139 kinetochore phenotype was observed in 60% of the Bik1-NES metaphase cells (Figure 3C). Line scan
140 analysis of the Ndc80-sfGFP fluorescence relative to the SPBs showed that Bik1-NES cells have a
141 flattened distribution of Ndc80 with kinetochores mispositioned towards the spindle equator (Figure
142 3D). Overall, the defects in kinetochore-clustering suggest that some kinetochore-microtubules are
143 abnormally long in Bik1-NES at metaphase.
144

145 ### Bik1 interacts with Cin8 at the spindle

146 Kinesin motor proteins have been shown to play an essential role in chromosome congression. To
147 investigate the overall interaction of Bik1 with kinesins, we performed single-step affinity purification
148 of Bik1-Flag in metaphase arrested cells, followed by mass spectrometry analysis. Bik1-Flag co-
149 purified with the yeast kinesins Kip2, Cin8, Kip1, Kip3 and Kar3 (Table 1). Noticeably, the kinesin Cin8
150 appeared with a similar coverage as the known interactor Kip2 (Supplementary data S1).
151

152 The defect of Bik1-NES cells in kinetochore clustering shown in Figure 3A phenocopies CIN8 deletion
153 (Gardner et al., 2008; Tytell & Sorger, 2006; Wargacki et al., 2010). Therefore, we decided to study
154 the Bik1-Cin8 interaction in more detail. We investigated whether Cin8 and Bik1 interact *in vivo* using
155 proximity-dependent biotin identification (TurboID), a proximity labelling assay that can detect
156 transient or weak protein-protein interactions (Roux et al., 2012). We fused TurboID, a mutated
157 version of a bacterial biotin ligase BirA (Branon et al., 2018; Larochelle et al., 2019), to the C-terminus
158 of Bik1 (Figure 4A). We then Flag-tagged Cin8 or Kip2, a kinesin known to interact with Bik1 at astral
159 microtubules (Carvalho et al., 2004). Both Cin8 and Kip2 were recovered after streptavidin pulldown
160 when expressed in Bik1-TurboID cells, indicating that Bik1 and Cin8 are in proximity *in vivo* (Figure
161 4B).
162
163 We next looked at the interaction between Bik1 and Cin8 in individual cells by bimolecular
164 fluorescence complementation (BiFC) (Sung & Huh, 2007). Briefly, an N-terminal fragment of the
165 yellow fluorescent protein Venus was fused to the C-terminus of Bik1, and a complimentary C-
166 terminal Venus fragment was fused to the C-terminus of Cin8. We detected BiFC signal at the spindle,
167 predominantly in metaphase and anaphase cells (Figure 4 C-D). Interestingly, the BiFC signal in
168 metaphase cells appeared as 1-2 dots close to the ends of the spindle, while the signal in anaphase
169 cells appeared as a single dot around the spindle midzone (Figure 4 C).
170
171 We then investigated the dependence of Cin8 and Bik1 to localize to the spindle. In the Bik1-NES
172 mutant, Cin8 still forms two foci between SPBs and kinetochores (Figure 5A and B), even in cells with
173 unclustered kinetochores. This result was surprising as Cin8 has been shown to bind kinetochores
174 directly (Suzuki et al., 2018). Linescan analysis of Cin8-sfGFP localization in relation to SPBs showed
175 that Cin8 localization is unaltered in the absence of nuclear Bik1 (Figure 5B). Deletion of CIN8, on the
176 other hand, resulted in a significantly reduced Bik1 intensity at the spindle (Figure 5C). Overall, these

177 data suggest that a portion of nuclear Bik1 associates with and is dependent on Cin8 to bind the
178 spindle.
179

180 Discussion

181 Our results demonstrate that the +TIP protein Bik1 – the yeast homolog of CLIP-170 – is critical for
182 chromosome congression.
183
184 We have shown that nuclear Bik1 localizes to kinetochores from G1 to metaphase, when it presents a
185 bilobed distribution like the pattern of the kinesins Cin8, Kip1, and Kip3 (Gardner et al., 2008; Tytell &
186 Sorger, 2006; Wargacki et al., 2010). Similar to these kinesins, Bik1 stays at kinetochores until
187 anaphase, when it concentrates at interpolar microtubules.
188
189 We explored the functions of Bik1 at the mitotic spindle using a Bik1-NES mutant, which preserves
190 Bik1 localization at astral microtubules and its role in spindle positioning, revealing phenotypes that
191 would have been difficult to interpret in a deletion mutant. Bik1-NES cells have a slower cell cycle
192 progression, characterized by a longer metaphase. Others have shown that Bik1 is needed to
193 nucleate microtubules that capture kinetochores after centromere re-activation (Tanaka et al., 2005).
194 Thus, Bik1's function in kinetochore capture could contribute to the cell cycle delay we observe.
195 However, we do not detect unattached kinetochores in the Bik1-NES mutant. Instead, the
196 kinetochores are aligned in the spindle but unclustered in a high percentage (60%) of metaphase
197 cells. Therefore, we hypothesize that the defect in chromosome congression is the main cause of the
198 metaphase delay.
199
200 Previous studies have shown that the kinesins Cin8 and to a lesser extent Kip1 and Kip3 are required
201 for yeast chromosome congression (Gardner et al., 2008; Tytell & Sorger, 2006; Wargacki et al.,

202 2010). However, the deletion of each kinesin results in different types of clustering defects. In the
203 *cin8Δ* mutant, the kinetochores move closer to the spindle equator (Gardner et al., 2008; Tytell &
204 Sorger, 2006; Wargacki et al., 2010). The *kip1Δ* mutant has a similar, but weaker, phenotype
205 (Gardner et al., 2008; Tytell & Sorger, 2006). Conversely, *kip3Δ* mutant cells mislocalize the
206 kinetochores towards the poles (Wargacki et al., 2010). Ndc80 clusters in the Bik1-NES mutant
207 appear shifted towards the spindle equator (Figure 3D), as has been reported for cin8Δ, suggesting
208 they perform similar functions at the kinetochores.
209
210 We have also shown that Bik1 associates with Cin8 at microtubules *in vivo*, using proximity-
211 dependent assays, in metaphase and anaphase. Furthermore, we found that the spindle associated
212 Bik1 is severely decreased in *cin8Δ*. The reduced Bik1 recruitment to the spindle and kinetochores
213 explains why Bik1 cannot compensate for the lack of Cin8, which is known to cause severe defects in
214 assembling the mitotic spindle (Hoyt et al., 1992; Kotwaliwale et al., 2007). A previous study has
215 shown that Cin8 mediates chromosome congression by depolymerizing kinetochore microtubules in
216 a length-dependent manner (Gardner et al., 2008). Gardner and coworkers proposed that Cin8 binds
217 randomly to kinetochore microtubules and walks towards the plus-end to promote microtubule plus-
218 end disassembly directly. However, in Bik1-NES cells, Cin8 is insufficient to regulate chromosome
219 congression. Moreover, Cin8 does not localize to the unclustered kinetochores in Bik1-NES. Taken
220 together, these observations suggest that Bik1 is a binding partner of Cin8 that contributes to the
221 disassembly of microtubule plus-ends to facility chromosome congression at metaphase. There are at
222 least two other examples where plus-end directed kinesin motors transport Bik1 in the cells. Kip2
223 transports Bik1 to astral microtubule plus ends to ensure proper spindle alignment (Carvalho et al.,
224 2004; Caudron et al., 2008). Furthermore, it has been suggested that Bik1 forms a complex with the
225 kinesin Kip3 during mating to induce microtubule depolymerization for nuclear congression (Molk et
226 al., 2006).
227

228 An important, but unanswered, question is how Bik1 regulates the dynamics of kinetochore
229 microtubules plus-end at the molecular level. One possibility is that Bik1 directly promotes
230 kinetochore-microtubule depolymerization. *In vitro* microtubule polymerization assays have shown
231 that Bik1 inhibits microtubule polymerization (Blake-Hodek et al., 2010). In that *in vitro* experimental
232 setup, however, Bik1 did not bind the microtubule ends, and therefore the authors proposed that
233 Bik1 could sequester free tubulin subunits, thereby limiting the rate of microtubule growth.
234
235 Another possibility is that Bik1 increases the processivity of Cin8. Bik1 has been proposed to act as a
236 processivity factor for the kinesin Kip2 at astral microtubules (Hibbel et al., 2015). Likewise, Bik1
237 might be needed for Cin8 to reach the plus-ends of long kinetochore microtubules that extend
238 beyond bundled kinetochore microtubules. Cin8 is a bidirectional kinesin and has been shown to
239 preferentially move in a minus-end directed manner as single motors (Gerson-Gurwitz et al., 2011;
240 Pandey et al., 2021; Roostalu et al., 2011). Directional switching has been shown to occur when Cin8
241 motors are clustered (Pandey et al., 2021; Roostalu et al., 2011), and other kinesin-5 motors switch
242 directionality in response to steric crowding on MTs (Britto et al., 2016). It is possible that loss of Bik1
243 leads to ineffective plus-end directed movement of Cin8 on long kinetochore microtubules.
244
245 In summary, we propose that that Bik1 and Cin8 collaborate to depolymerize long kinetochore-
246 microtubules to promote kinetochore clustering.
247

248 Materials and Methods

249 Yeast strains and plasmids

250 All *S. cerevisiae* strains used in this study are derivatives of BY4741 and are listed in Table S1. The
251 epitope tagged alleles (sfGFP and tagRFPT), TurboID-3xmyc and BiFC were constructed at the
252 endogenous loci by standard PCR-based integration as described in (Longtine et al., 1998) and

253 confirmed by PCR, sequencing and microscopy. The plasmids used to generate the strains are listed
254 in Table S2. Strains with fluorescently tagged Tub1 were constructed as described in (Markus et al.,
255 2015). Briefly, the listed plasmids were linearized using BsaBI (New England Biolabs, R0537S). The
256 linearized plasmid was then integrated by at the endogenous TUB1 locus.
257

258 ## Growth conditions

259 Cells were grown at 30°C in YEP (1% yeast extract, 2% bacto-peptone) medium supplemented with
260 2% glucose (YEPD) unless otherwise stated. For G1 arrest, overnight cultures were diluted to OD_{600} =
261 0.1 in fresh media, grown for 2.5 hours and arrested by adding 3 µg/ml α-factor (Sigma, custom
262 peptide WHWLQLKPGQPMY) every 60 min for 120 min. Cells were released by washing away α-factor
263 with 1x culture volume of YEPD, resuspending in 1x culture volume of YEPD, and further grown at
264 30°C. For metaphase arrest, PGal1-Cdc20 cells were grown in YEP supplemented with 2% raffinose
265 and 2% galactose, and switched to YEPD for 120 min.
266

267 ## Fluorescence imaging

268 Cells were fixed in 4% formaldehyde on ice for 60 minutes, washed with PBS and stored in PBS at 4°C
269 until imaging. Cells were imaged in concanavalin A-coated 96 well glass bottom plates. Images were
270 acquired using a Nikon Ti microscope, equipped with a Zyla 4.2+ sCMOS camera and a 60x water
271 immersion objective (NA 1.2). Z-stack images (4-8 µm, 0.3 µm steps) were captured for fixed cells.
272 Images for BiFC and immunofluorescence were acquired using a Nikon Ti2 microscope, equipped
273 with a Prime BSI sCMOS camera and a 60x water immersion objective (NA 1.2).
274

275 ## Live-cell imaging

276 Cells were arrested in G1 as described. Arrested cells were released in low-fluorescence media (LFM)
277 containing 1.7 g/l yeast nitrogen base without ammonium sulfate, amino acids, folic acid and
278 riboflavin (MP-Biomedicals, 4030-512), and 1 g/l monosodium glutamate, supplemented with 2%

279 glucose and amino acids. Cells were left to settle on the bottom of concanavalin A-coated 96 well
280 glass bottom plates for 20-30 minutes inside the microscope incubator at 30°C before being imaged.
281 Images were captured every 5 min for 100-120 min.
282

283 ## Image analysis

284 Fluorescence intensity measurements were made from maximum intensity projections of image z-
285 stacks using FiJi (Schindelin et al., 2012). Integrated intensities were measured in a region of interest
286 drawn around spindles/kinetochores. Background correction was done by multiplying the mean
287 fluorescence of regions outside of the nucleus with the measured region's area and subtracting from
288 the measured integrated intensity.
289

290 Linescan analysis was performed by drawing a line between the centers of opposing SPB foci and
291 measuring the fluorescence intensities along the line. Background correction was done by
292 subtracting the mean fluorescence measured at the cytoplasm. Binned means were calculated for
293 each strain.
294

295 ## Immunofluorescence

296 PGal1-Cdc20 cells were arrested in metaphase and fixed by adding formaldehyde to 3.7% (vol/vol)
297 and incubating while shaking at 30°C for 30 min. The fixed cells were washed once with PBS and then
298 twice with SP buffer (0.1 M KPO4, 1.2 M sorbitol, pH 7.5). The cells were resuspended in 500 µl SP
299 buffer with 0.1% β-mercaptoethanol and 10 µl of 20 mg/ml Zymoylase-20T (Seikagaku). The cells
300 were incubated with soft rotation for 20 min at room temperature (RT). The resulting spheroplasts
301 were then washed twice in SP buffer and permeabilized in blocking solution (3% BSA 0.1% Triton X-
302 100 in PBS) for 30 min at RT. The spheroplasts were immunostained in suspension. First, cells were
303 incubated with 1:1000 mouse monoclonal anti-FLAG M2 antibody (Sigma, F1804) in blocking buffer
304 for 1 hour at RT. Cells were washed three times in PBS and then incubated with 1:100 donkey anti-

305 mouse Alexa Fluor 647 antibody (ThermoFisher, A-31571) for 45 min at RT. Cells were washed three
306 times in PBS, seed in a glass-bottom imaging plate coated with Concanavalin A, and imaged.
307

308 ## Sample preparation for mass spectrometry analysis

309 Bik1-5xFlag PGal1-Cdc20 cells were arrested in metaphase. Briefly, cells were grown overnight in 50
310 ml YEP with 2% galactose and 2% raffinose. Cells were diluted in 2 L YEP with 2% and 2% raffinose
311 and grown at 30°C to OD_{600} = 1. Then, cells were spun down and resuspended in 2 L YEPD with 2%
312 glucose and arrested at 30°C for 2 h. Cells were spun down at 6000 rom at 4°C, washed with cold
313 dH_2O, and spun down at 6000 rpm at 4°C. The cell pellet was diluted in a few drops of lysis buffer (50
314 mM Tris, pH 8.0, 150 mM NaCl, 5% glycerol, 0.1% Triton X-100). The cell suspension was snap frozen
315 by pipetting the drops directly into liquid nitrogen. The frozen pellets were then lysed using a
316 Freezer/Mill (SPEX™ sample prep freezer/mill), using 10 rounds consisting of 2 min grinding at 14
317 rpm, 2 min cooling). The yeast pellets were diluted in buffer EB1 (40 mM sodium hepes, 300 mM
318 NaCl, 0.5% Triton X-100, 2 mM $MgCl_2$, 5% glycerol and protease and phosphatase inhibitors (1mM
319 PMSF, 1mM leupeptin, 1mM peptasin A, 10mM NaF, 1mM sodium pyrophosphatase, 1mm sodium
320 orthovanadate), and clarified by centrifugation at 10 000 g for 10 min at 4 °C. The cleared lysate was
321 incubated for 30 min with magnetic Dynabeads (Thermo Fisher Scientific) coupled with anti-FLAG M2
322 antibody (Sigma-Aldrich). The Dynabeads were washed three times with buffer A (25 mM sodium
323 Hepes, 2 mM $MgCl_2$, 0.1% EDTA, 0.1% Triton X-100, 5% glycerol, 150 mM NaCl, protease and
324 phosphatase inhibitors (1 mM PMSF, 1 mM leupeptin, 1 mM peptasin A, 10mM NaF, 1 mM sodium
325 pyrophosphatase, 1 mm sodium orthovanadate) and four times with buffer B (25 mM Hepes, pH 8.0,
326 and 150 mM KCl).
327

328 ## Protein on-beads digestion

329 Proteins bound to the Dynabeads were resuspended and washed with 500 µL of 50 mM ammonium
330 bicarbonate (AmBic), pH 8.0, twice. After incubation at room temperature for 15 min, 50 µL of 50

331 mM AmBic was added. Protein disulfide bonds were reduced with 5 µL of 200 mM dithiothreitol at
332 37°C for 45 min and alkylated with 5 µL of 600 mM iodoacetamide at room temperature in dark for
333 30 min. Tryptic digestion was started by adding 1 µg of trypsin and incubation at 37°C overnight,
334 followed by adding another 500 ng of trypsin and incubation at 30°C for 3 h. The digestion was
335 stopped with 5 µL concentrated formic acid. The samples were then cleaned on a C18 StageTip
336 (Thermo Scientific) and dried using a speedvac (MiVac, Thermo Scientific).
337

338 ## PRLC-MS/MS analysis

339 Chromatographic separations of peptides were performed on a 50 cm long C18 EASY-spray column
340 connected to an Easy nanoLC-1000 UPLC system (Thermo Fisher Scientific). The gradient was 4-25%
341 of solvent B (98% acetonitrile, 0.1% formic acid) in 50 min and 25-40%B in 10 min at a flow rate of
342 300 nL/min. An Orbitrap Fusion mass spectrometer (Thermo Scientific) analyzed the eluted peptides
343 that were ionized in a nano-Easy electrospray source. The survey mass spectrum was acquired at the
344 resolution of 120,000 in the range of *m/z* 350-1800. MS/MS data of precursors were obtained with
345 30% normalized collision energy by higher-energy collisional dissociation (HCD) for ions with charge
346 *z*=2-7 at a resolution of 30,000 in 3 s cycle time.
347

348 ## Data analysis

349 Mascot v 2.5.1 search engine (MatrixScience Ltd., UK) was used for protein identification with the
350 following search parameters: up to two missed cleavage sites for trypsin, peptide mass tolerance 10
351 ppm, 0.05 Da for the HCD fragment ions. Carbamidomethylation of cysteine was specified as a fixed
352 modification, whereas oxidation of methionine, deamidation of asparagine and glutamine were
353 defined as variable modifications.
354

355 Turbo-ID assay

356 Overnight cultures were diluted to OD_{600} = 0.2 in YEPD medium supplemented with 50 µM biotin and
357 grown at 30°C until they reached OD_{600} = 0.6 (4-5 h). Cells were pelleted and resuspended in RIPA
358 buffer (50 mM Tris-HCl, 150 mM NaCl, 1 mM EDTA, 0.1% SDS, 1% Triton X-100, 1.5 mM MgCl2, 0.4%
359 sodium deoxycholate, 1 mM DTT, 1 mM PMSF, 1 mM leupeptin and1 mM pepstatin A). The cells
360 were lysed using acid-washed glass beads and a bead-beater at 4°. To shear the DNA and RNA, the
361 cell lysate was sonicated, and then clarified by centrifugation. Clarified lysates were incubated with
362 100 µl of Streptavidin-Sepharose beads (GE Healthcare; 17-5113-01) for 3 h at 40°C. The beads were
363 then washed once with wash buffer (50mM Tris-HCl, 2% SDS) and three times with RIPA buffer. The
364 purified proteins were eluted with 4 x Laemmli buffer containing 25 µM biotin and 10% β-
365 mercaptoethanol, for 15 min at 95°C. The whole cell extract or pull-down samples were separated by
366 SDS-PAGE, and the proteins were transferred to a PVDF membrane (BioRad) followed by and
367 standard immunoblotting. Primary (monoclonal anti-FLAG M2 antibody (Sigma-Aldrich, F3165,
368 diluted 1:5000); c-Myc rabbit polyclonal antibody (Santa Cruz Biotechnology; sc-789, diluted 1:5000);
369 anti-Pgk1 mouse monoclonal antibody (Invitrogen, 45925, diluted 1:5000), and secondary anti-
370 mouse IgG peroxidase antibody, (Sigma, A9044, diluted 1:50000) were used. HRP conjugated
371 secondary antibodies were detected with Femto ECL (ThermoFisher Scientific).
372

373 # Acknowledgements

374 We thank C. Björkegren (Karolinska Institutet, Sweden) for reagents, and C. Boone and Z. Li for help
375 with construction of deletion mutants and critical reading of this manuscript. Microscopy was
376 performed at the LCI facility/Nikon Center of Excellence, Karolinska Institutet, supported by grants
377 from the Knut and Alice Wallenberg Foundation, Swedish Research Council, KI infrastructure, Centre
378 for Innovative Medicine and Jonasson center at the Royal Institute of Technology. Protein
379 identification and quantification were carried out by the Proteomics Biomedicum core facility,

380 Karolinska Institutet. This work was supported by grants from the Swedish Council (VR-NT 2017-
381 04536), and STINT (Mobility Grant for Internationalization, MG2019-8484) to V.M.B. The authors
382 declare no competing financial interests.
383

384 ## References

385 Akhmanova, A., & Steinmetz, M. O. (2010). Microtubule +TIPs at a glance. In *Journal of Cell Science*
386 (Vol. 123, Issue 20). https://doi.org/10.1242/jcs.062414
387 Berlin, V., Styles, C. A., & Fink, G. R. (1990). BIK1, a protein required for microtubule function during
388 mating and mitosis in Saccharomyces cerevisiae, colocalizes with tubulin. *Journal of Cell Biology*,
389 *111*(6 I). https://doi.org/10.1083/jcb.111.6.2573
390 Blake-Hodek, K. A., Cassimeris, L., & Huffaker, T. C. (2010). Regulation of microtubule dynamics by
391 Bim1 and Bik1, the budding yeast members of the EB1 and CLIP-170 families of plus-end
392 tracking proteins. *Molecular Biology of the Cell*, *21*(12). https://doi.org/10.1091/mbc.E10-02-
393 0083
394 Branon, T. C., Bosch, J. A., Sanchez, A. D., Udeshi, N. D., Svinkina, T., Carr, S. A., Feldman, J. L.,
395 Perrimon, N., & Ting, A. Y. (2018). Efficient proximity labeling in living cells and organisms with
396 TurboID. *Nature Biotechnology*, *36*(9). https://doi.org/10.1038/nbt.4201
397 Britto, M., Goulet, A., Rizvi, S., Von Loeffelholz, O., Moores, C. A., & Cross, R. A. (2016).
398 Schizosaccharomyces pombe kinesin-5 switches direction using a steric blocking mechanism.
399 *Proceedings of the National Academy of Sciences of the United States of America*, *113*(47).
400 https://doi.org/10.1073/pnas.1611581113
401 Carvalho, P., Gupta, M. L., Hoyt, M. A., & Pellman, D. (2004). Cell cycle control of kinesin-mediated
402 transport of Bik1 (CLIP-170) regulates microtubule stability and dynein activation.
403 *Developmental Cell*, *6*(6). https://doi.org/10.1016/j.devcel.2004.05.001
404 Caudron, F., Andrieux, A., Job, D., & Boscheron, C. (2008). A new role for kinesin-directed transport of

405 Bik1p (CLIP-170) in Saccharomyces cerevisiae. *Journal of Cell Science*, *121*(9).
406 https://doi.org/10.1242/jcs.023374
407 Gardner, M. K., Bouck, D. C., Paliulis, L. V., Meehl, J. B., O'Toole, E. T., Haase, J., Soubry, A., Joglekar,
408 A. P., Winey, M., Salmon, E. D., Bloom, K., & Odde, D. J. (2008). Chromosome Congression by
409 Kinesin-5 Motor-Mediated Disassembly of Longer Kinetochore Microtubules. *Cell*, *135*(5).
410 https://doi.org/10.1016/j.cell.2008.09.046
411 Gardner, M. K., Pearson, C. G., Sprague, B. L., Zarzar, T. R., Bloom, K., Salmon, E. D., & Odde, D. J.
412 (2005). Tension-dependent Regulation of Microtubule Dynamics at Kinetochores Can Explain
413 Metaphase Congression in Yeast. *Molecular Biology of the Cell*, *16*(8), 3764–3775.
414 https://doi.org/10.1091/mbc.e05-04-0275
415 Gerson-Gurwitz, A., Thiede, C., Movshovich, N., Fridman, V., Podolskaya, M., Danieli, T., Lakämper, S.,
416 Klopfenstein, D. R., Schmidt, C. F., & Gheber, L. (2011). Directionality of individual kinesin-5 Cin8
417 motors is modulated by loop 8, ionic strength and microtubule geometry. *EMBO Journal*,
418 *30*(24). https://doi.org/10.1038/emboj.2011.403
419 Hibbel, A., Bogdanova, A., Mahamdeh, M., Jannasch, A., Storch, M., Schäffer, E., Liakopoulos, D., &
420 Howard, J. (2015). Kinesin Kip2 enhances microtubule growth in vitro through length-
421 dependent feedback on polymerization and catastrophe. *ELife*, *4*(NOVEMBER2015).
422 https://doi.org/10.7554/eLife.10542
423 Hoyt, M. A., He, L., Kek Khee Loo, & Saunders, W. S. (1992). Two Saccharomyces cerevisiae kinesin-
424 related gene products required for mitotic spindle assembly. *Journal of Cell Biology*, *118*(1).
425 https://doi.org/10.1083/jcb.118.1.109
426 Kops, G. J. P. L., Saurin, A. T., & Meraldi, P. (2010). Finding the middle ground: How kinetochores
427 power chromosome congression. In *Cellular and Molecular Life Sciences* (Vol. 67, Issue 13).
428 https://doi.org/10.1007/s00018-010-0321-y
429 Kosugi, S., Hasebe, M., Tomita, M., & Yanagawa, H. (2008). Nuclear export signal consensus
430 sequences defined using a localization-based yeast selection system. *Traffic*, *9*(12).

431 https://doi.org/10.1111/j.1600-0854.2008.00825.x

432 Kotwaliwale, C. V., Frei, S. B., Stern, B. M., & Biggins, S. (2007). A Pathway Containing the Ipl1/Aurora
433 Protein Kinase and the Spindle Midzone Protein Ase1 Regulates Yeast Spindle Assembly.
434 *Developmental Cell*, *13*(3). https://doi.org/10.1016/j.devcel.2007.07.003

435 Larochelle, M., Bergeron, D., Arcand, B., & Bachand, F. (2019). Proximity-dependent biotinylation
436 mediated by TurboID to identify protein-protein interaction networks in yeast. *Journal of Cell*
437 *Science*, *132*(11). https://doi.org/10.1242/jcs.232249

438 Lin, H., De Carvalho, P., Kho, D., Tai, C. Y., Pierre, P., Fink, G. R., & Pellman, D. (2001). Polyploids
439 require Bik1 for kinetochore-microtubule attachment. *Journal of Cell Biology*, *155*(7).
440 https://doi.org/10.1083/jcb.200108119

441 Longtine, M. S., McKenzie, A., Demarini, D. J., Shah, N. G., Wach, A., Brachat, A., Philippsen, P., &
442 Pringle, J. R. (1998). Additional modules for versatile and economical PCR-based gene deletion
443 and modification in Saccharomyces cerevisiae. *Yeast*, *14*(10).
444 https://doi.org/10.1002/(SICI)1097-0061(199807)14:10<953::AID-YEA293>3.0.CO;2-U

445 Maiato, H., Gomes, A. M., Sousa, F., & Barisic, M. (2017). Mechanisms of chromosome congression
446 during mitosis. In *Biology* (Vol. 6, Issue 1). https://doi.org/10.3390/biology6010013

447 Marco, E., Dorn, J. F., Hsu, P. H., Jaqaman, K., Sorger, P. K., & Danuser, G. (2013). S. cerevisiae
448 chromosomes biorient via gradual resolution of syntely between S phase and anaphase. *Cell*,
449 *154*(5). https://doi.org/10.1016/j.cell.2013.08.008

450 Markus, S. M., Omer, S., Baranowski, K., & Lee, W. L. (2015). Improved Plasmids for Fluorescent
451 Protein Tagging of Microtubules in Saccharomyces cerevisiae. *Traffic*, *16*(7).
452 https://doi.org/10.1111/tra.12276

453 Miller, R. K., D'Silva, S., Moore, J. K., & Goodson, H. V. (2006). The CLIP-170 Orthologue Bik1p and
454 Positioning the Mitotic Spindle in Yeast. In *Current Topics in Developmental Biology* (Vol. 76).
455 https://doi.org/10.1016/S0070-2153(06)76002-1

456 Molk, J. N., Salmon, E. D., & Bloom, K. (2006). Nuclear congression is driven by cytoplasmic

457 microtubule plus end interactions in S. cerevisiae. *Journal of Cell Biology*, *172*(1).
458 https://doi.org/10.1083/jcb.200510032
459 Moore, J. K., D'Silva, S., & Miller, R. K. (2006). The CLIP-170 homologue Bik1p promotes the
460 phosphorylation and asymmetric localization of Kar9p. *Molecular Biology of the Cell*, *17*(1).
461 https://doi.org/10.1091/mbc.E05-06-0565
462 O'Toole, E. T., Winey, M., & McIntosh, J. R. (1999). High-voltage electron tomography of spindle pole
463 bodies and early mitotic spindles in the yeast Saccharomyces cerevisiae. *Molecular Biology of*
464 *the Cell*, *10*(6). https://doi.org/10.1091/mbc.10.6.2017
465 Pandey, H., Reithmann, E., Goldstein-Levitin, A., Al-Bassam, J., Frey, E., & Gheber, L. (2021). Drag-
466 induced directionality switching of kinesin-5 Cin8 revealed by cluster-motility analysis. *Science*
467 *Advances*, *7*(6). https://doi.org/10.1126/sciadv.abc1687
468 Pearson, C. G., Gardner, M. K., Paliulis, L. V., Salmon, E. D., Odde, D. J., & Bloom, K. (2006). Measuring
469 nanometer scale gradients in spindle microtubule dynamics using model convolution
470 microscopy. *Molecular Biology of the Cell*, *17*(9). https://doi.org/10.1091/mbc.E06-04-0312
471 Peterson, J. B., & Ris, H. (1976). Electron microscopic study of the spindle and chromosome
472 movement in the yeast Saccharomyces cerevisiae. *Journal of Cell Science*, *22*(2).
473 Powers, A. F., Franck, A. D., Gestaut, D. R., Cooper, J., Gracyzk, B., Wei, R. R., Wordeman, L., Davis, T.
474 N., & Asbury, C. L. (2009). The Ndc80 Kinetochore Complex Forms Load-Bearing Attachments to
475 Dynamic Microtubule Tips via Biased Diffusion. *Cell*, *136*(5).
476 https://doi.org/10.1016/j.cell.2008.12.045
477 Roberts, A. J., Goodman, B. S., & Reck-Peterson, S. L. (2014). Reconstitution of dynein transport to
478 the microtubule plus end by kinesin. *ELife*, *3*. https://doi.org/10.7554/elife.02641
479 Roostalu, J., Hentrich, C., Bieling, P., Telley, I. A., Schiebel, E., & Surrey, T. (2011). Directional
480 switching of the kinesin Cin8 through motor coupling. *Science*, *332*(6025).
481 https://doi.org/10.1126/science.1199945
482 Roux, K. J., Kim, D. I., Raida, M., & Burke, B. (2012). A promiscuous biotin ligase fusion protein

483 identifies proximal and interacting proteins in mammalian cells. *Journal of Cell Biology*, *196*(6).
484 https://doi.org/10.1083/jcb.201112098
485 Schindelin, J., Arganda-Carreras, I., Frise, E., Kaynig, V., Longair, M., Pietzsch, T., Preibisch, S., Rueden,
486 C., Saalfeld, S., Schmid, B., Tinevez, J. Y., White, D. J., Hartenstein, V., Eliceiri, K., Tomancak, P., &
487 Cardona, A. (2012). Fiji: An open-source platform for biological-image analysis. In *Nature*
488 *Methods* (Vol. 9, Issue 7). https://doi.org/10.1038/nmeth.2019
489 Sprague, B. L., Pearson, C. G., Maddox, P. S., Bloom, K. S., Salmon, E. D., & Odde, D. J. (2003).
490 Mechanisms of microtubule-based kinetochore positioning in the yeast metaphase spindle.
491 *Biophysical Journal*, *84*(6). https://doi.org/10.1016/S0006-3495(03)75087-5
492 Su, X., Qiu, W., Gupta, M. L., Pereira-Leal, J. B., Reck-Peterson, S. L., & Pellman, D. (2011).
493 Mechanisms Underlying the Dual-Mode Regulation of Microtubule Dynamics by Kip3/Kinesin-8.
494 *Molecular Cell*, *43*(5). https://doi.org/10.1016/j.molcel.2011.06.027
495 Sung, M. K., & Huh, W. K. (2007). Biomolecular fluorescence complementation analysis system for in
496 vivo detection of protein-protein interaction in Saccharomyces cerevisiae. *Yeast*, *24*(9).
497 https://doi.org/10.1002/yea.1504
498 Suzuki, A., Badger, B. L., Haase, J., Ohashi, T., Erickson, H. P., Salmon, E. D., & Bloom, K. (2016). How
499 the kinetochore couples microtubule force and centromere stretch to move chromosomes.
500 *Nature Cell Biology*, *18*(4). https://doi.org/10.1038/ncb3323
501 Suzuki, A., Gupta, A., Long, S. K., Evans, R., Badger, B. L., Salmon, E. D., Biggins, S., & Bloom, K. (2018).
502 A Kinesin-5, Cin8, Recruits Protein Phosphatase 1 to Kinetochores and Regulates Chromosome
503 Segregation. *Current Biology*, *28*(17). https://doi.org/10.1016/j.cub.2018.08.038
504 Tanaka, K., Mukae, N., Dewar, H., Van Breugel, M., James, E. K., Prescott, A. R., Antony, C., & Tanaka,
505 T. U. (2005). Molecular mechanisms of kinetochore capture by spindle microtubules. *Nature*,
506 *434*(7036). https://doi.org/10.1038/nature03483
507 Tytell, J. D., & Sorger, P. K. (2006). Analysis of kinesin motor function at budding yeast kinetochores.
508 *Journal of Cell Biology*, *172*(6). https://doi.org/10.1083/jcb.200509101

Varga, V., Helenius, J., Tanaka, K., Hyman, A. A., Tanaka, T. U., & Howard, J. (2006). Yeast kinesin-8 depolymerizes microtubules in a length-dependent manner. *Nature Cell Biology*, *8*(9). https://doi.org/10.1038/ncb1462

Wargacki, M. M., Tay, J. C., Muller, E. G., Asbury, C. L., & Davis, T. N. (2010). Kip3, the yeast kinesin-8, is required for clustering of kinetochores at metaphase. *Cell Cycle*, *9*(13). https://doi.org/10.4161/cc.9.13.12076

Winey, M., Mamay, C. L., O'Toole, E. T., Mastronarde, D. N., Giddings, T. H., McDonald, K. L., & McIntosh, J. R. (1995). Three-dimensional ultrastructural analysis of the Saccharomyces cerevisiae mitotic spindle. *Journal of Cell Biology*, *129*(6). https://doi.org/10.1083/jcb.129.6.1601

Winey, M., & O'Toole, E. T. (2001). The spindle cycle in budding yeast. In *Nature Cell Biology* (Vol. 3, Issue 1). https://doi.org/10.1038/35050663

Xiang, X. (2018). Nuclear movement in fungi. In *Seminars in Cell and Developmental Biology* (Vol. 82). https://doi.org/10.1016/j.semcdb.2017.10.024

525 ## Figure Legends

526 **Figure 1. Bik1 localizes to kinetochores in a cell-cycle dependent manner. (A)** Representative images
527 of Bik1-sfGFP (green) localization in cycling cells expressing mTurquoise-Tub1 (blue) and Spc42-
528 tagRFP-T (red, top panel), and Nc80-tagRFP-T (red, lower panel). **(B)** Top panel: Representative
529 images of Bik1-sfGFP (green) localization in pGal1-Cdc20 metaphase-arrested cells expressing Nc80-
530 tagRFP-T. Lower panel: Line scan analysis shows the distribution of Bik1-sfGFP and kinetochores
531 (Ndc80-tagRFP-T) in metaphase arrested cells. The fluorescence intensity was measured along lines
532 drawn between the kinetochore foci and normalized relative to the maximum values, and mean
533 values are shown (n=26 cells). **(C)** Cartoon showing the design of Bik1-NES. In short, a strong nuclear
534 export signal (NES) was fused to Bik1-sfGFP or Bik1-5xFlag to promote nuclear export. **(D)**
535 Representative images of Bik1-sfGFP-NES (green) localization in cycling cells expressing mTurquoise-
536 Tub1 (blue) and Ndc80-tagRFPT (red). **(E)** Quantification of Bik1-sfGFP or Bik1-sfGFP-NES localization
537 in metaphase cells. Bik1-sfGFP and Bik1-sfGFP-NES cells expressing mRuby2-Tub1 were arrested in
538 G1 with α-factor and subsequently released in fresh media. Cells were fixed every 10 minutes for 120
539 minutes. Left: Representative cells at metaphase. Time after release = 40 min (Bik1-sfGFP), and 50
540 min (Bik1-sfGFP-NES). Right: Boxplots of the integrated fluorescence intensity of Bik1-sfGFP and Bik1-
541 sfGFP-NES at the spindle (mRuby2-Tub1) in metaphase cells (n=55 cells). All images shown are
542 maximum intensity projections of Z-stacks (9 µm, 1 µm steps). Dashed lines represent the cell
543 outlines based on bright field images. Scale bars: 4 µm.
544

545 **Figure 2. Bik1-NES delays spindle elongation at metaphase/anaphase transition. (A)** Cells from (1E)
546 were scored for cell cycle progression based on bud size and spindle length (mRuby-Tub1). Means of
547 3 independent experiments are shown (n=100 cells each). Error bars SD. **(B-E)** Time-lapse imaging of
548 cells expressing Bik1-sfGFP or Bik1-sfGFP-NES (green) and Ndc80-tagRFP-T (red). Cells were arrested
549 in G1 with α-factor, subsequently released in fresh medium under the microscope. Images were
550 taken at 5 min intervals. **(B)** Representative time-lapse images. Arrowheads indicate the appearance

551 of separated kinetochore clusters. Arrows indicate segregated kinetochores in mother/bud. The time
552 (min) elapsed from appearance of separated kinetochore clusters is indicated by the numbers above
553 the frames. Images shown are maximum intensity projections of Z-stacks (9 µm, 1 µm steps). **(C)**
554 From the upper panel of Figure 2B, zoomed-in images of the kinetochores (Ndc80-tagRFP-T) at
555 metaphase and anaphase. **(D)** Boxplots of the integrated Bik1-sfGFP fluorescence intensity at
556 kinetochores (Ndc80-tagRFP-T) at metaphase (meta) and anaphase (ana) (n= 27 cells). **(E)**
557 Quantification of average time from the appearance of separated kinetochore clusters to segregated
558 kinetochores in mother/bud in Bik1-sfGFP and Bik1-sfGFP-NES cells from 2 independent experiments
559 (n = 57-59 cells). Error bars SD. p-value = 0.001691 using Welch Two Sample t-test.
560
561 **Figure 3. Nuclear Bik1 is needed for kinetochore clustering at metaphase. (A)** Representative
562 immunofluorescence staining for Bik1-5xFlag and Bik1-5xFlag-NES (magenta) in metaphase arrested
563 pGal1-Cdc20 cells expressing Spc42-sfGFP (red) and Ndc80-TagRFP-T (green). Images shown are
564 maximum intensity projections of Z-stacks (4.95 µm, 0.3 µm steps). **(B)** Representative images of
565 Bik1-5xFlag and Bik1-5xFlag-NES arrested as in (A), including zoomed-in images of the kinetochores
566 (Ndc80-sfGFP). Images shown are maximum intensity projections of Z-stacks (8.7 µm, 0.3 µm steps).
567 **(C)** Quantification of kinetochore (Ndc80-tagRFPT) unclustered phenotype in Bik1-5xFlag and Bik-
568 5xFlag-NES cells arrested in metaphase as shown in (B). Bar plots show means from 3 independent
569 experiments (n=100 cells each). Error bars, SD. p=0.0006884 using Welch Two Sample t-test **(D)** Line
570 scan analysis shows the distribution of kinetochores (Ndc80sfGFP) and spindle pole bodies (SPBs,
571 Spc42-tagRFP-T) in metaphase arrested cells. Fluorescence intensity was measured along lines drawn
572 between the SPBs (Spc42-TagRFP-T) and normalized relative to the maximum values, and mean
573 values are shown (n=100 cells). Scale bars: 4 µm.
574
575 **Figure 4. Bik1 interacts with Cin8 at metaphase (A-B)** Identification of Cin8 as a Bik1 interaction
576 partner using TurboID. Cartoon outlining the principle of the TurboID assay. Briefly, a biotin ligase

577 was fused to endogenous Bik1 (Bik1-TurboID) in cells expressing the protein of interest tagged with
578 Flag (Prey). Biotinylated substrates were purified using streptavidin beads, and inputs and pull-down
579 lysates were analyzed by immunoblot for the indicated proteins. **(B)** Western blot analysis of total
580 cell extracts (input) and streptavidin pull-downs prepared from Bik1-TurboID-3xmyc cells expressing
581 Kip2-5xFlag or Cin8-5xFlag as prey, and control strains, using anti-Myc (top) and anti-Flag (bottom)
582 antibodies. (*) unspecific band. **(C-D)** Bimolecular fluorescence complementation (BiFC) analysis of
583 Bik1 and Cin8 interaction. **(C)** Representative images of cycling cells expressing Bik1-VN and Cin8-VC
584 in G1, metaphase and anaphase. Images shown are single focal planes. **(D)** Proportion of cells in (C)
585 with BIFC signal based on Venus fluorescence (3 independent experiments, n=50 cells per
586 experiment and cell cycle stage). Error bars, SD.
587
588 **Figure 5. Dependence of Cin8 and Bik1 to localize to the spindle (A-B)** Cin8 localizes at the spindle in
589 Bik1-NES cells, but does not co-localize with unclustered kinetochores. **(A)** Cin8 localization at the
590 metaphase spindle does not require nuclear Bik1. Representative images of pGal1-Cdc20 cells
591 arrested in metaphase expressing Bik1-5xFlag or Bik1-5xFlag-NES, Cin8-sfGFP, and the markers
592 Ndc80-TagRFP-T (top panel) or Spc42-TagRFP-T (lower panel). Images shown are maximum intensity
593 projections of Z-stacks (8.7 µm, 0.3 µm steps). **(B)** Line scan analysis of Cin8 distribution (Cin8-sfGFP)
594 in metaphase arrested cells). Top panel: Cin8 distribution relative to the kinetochores (Ndc80-
595 tagRFP-T). The fluorescence intensity of Cin8-sfGFP and Ndc80-tagRFPT was measured along lines
596 drawn between the SPBs and normalized relative to the maximum values, mean values are shown
597 (n= 26 cells). Low panel: Cin8 distribution relative to the SPBs (Spc42-tagRFP-T). The fluorescence
598 intensity of Cin8-sfGFP and Spc42-tagRFPT was measured along lines drawn between the SPBs and
599 normalized relative to the maximum values. Mean values are shown (n= 26cells). **(C)** Cin8 is needed
600 for Bik1-sfGFP Bik1-sfGFP localization at kinetochores. CIN8 and cin8Δ cells expressing Bik1-sfGFP and
601 Ndc80-TagRFP-T were arrested in G1 using α-factor, released in fresh media at 25°C and fixed every
602 10 minutes for 130 minutes. Left: Representative images of cells in metaphase (CIN8, 60 min after

603 release; cin8Δ, 110 min after release) Images shown are maximum intensity projections of Z-stacks
604 (6.6 µm, 0.6 µm steps). Right: Boxplots of the integrated fluorescence intensity of Cin8-sfGFP at the
605 spindle (based on Ndc80-TagRFP-T localization) in metaphase cells (n=100 cells each). Scale bars: 4
606 µm.
607

Figure 1

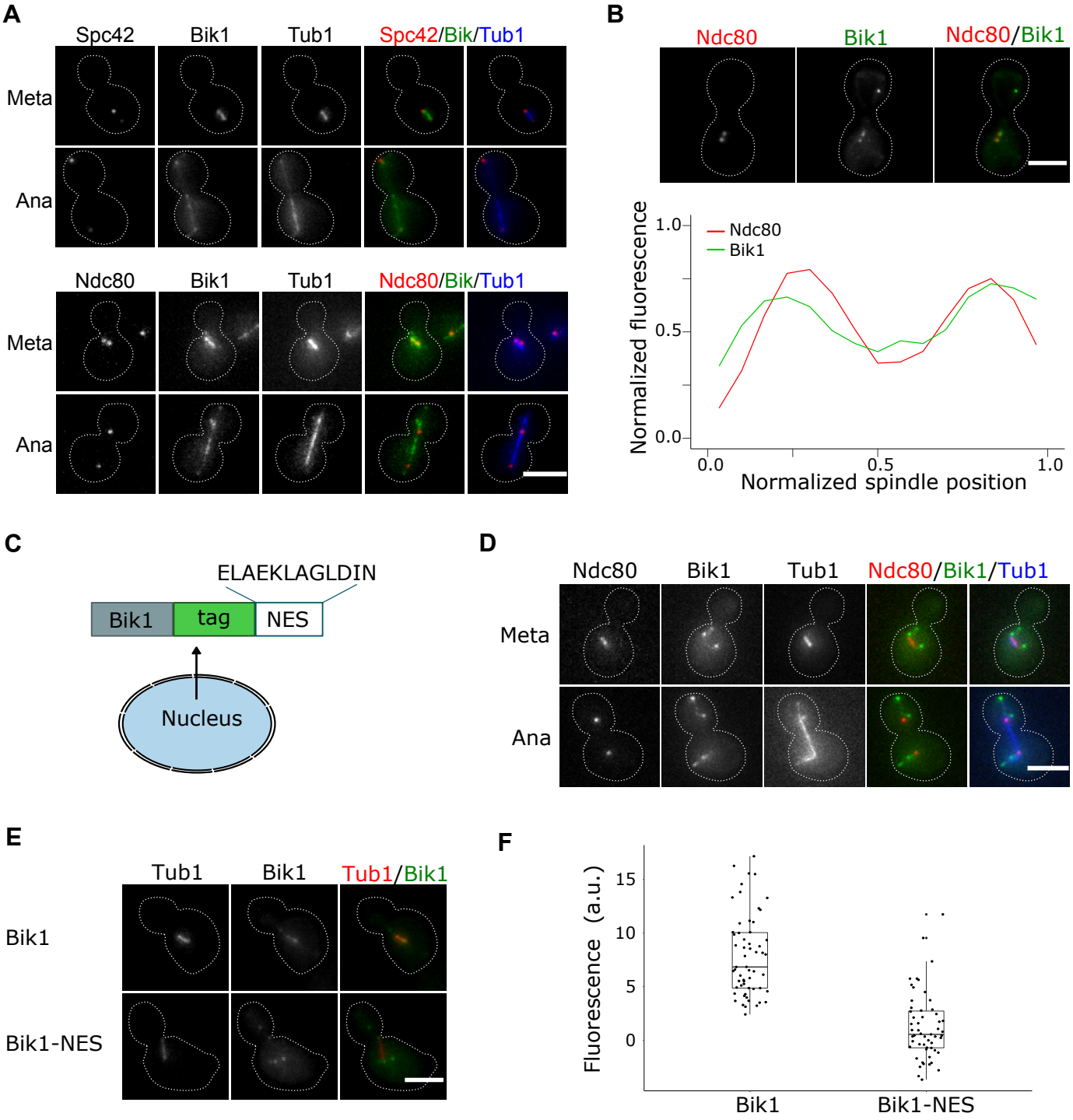
A
Spc42
Bik1
Tub1
Spc42/Bik/Tub1
Meta
Ana
Ndc80
Bik1
Tub1
Ndc80/Bik/Tub1
Meta
Ana
B
Ndc80
Bik1
Ndc80/Bik1
Ndc80
Bik1
Normalized fluorescence
1.0
0.5
0.0
0.0
0.5
1.0
Normalized spindle position
C
ELAEKLAGLDIN
Bik1
tag
NES
Nucleus
D
Ndc80
Bik1
Tub1
Ndc80/Bik1/Tub1
Meta
Ana
E
Tub1
Bik1
Tub1/Bik1
Bik1
Bik1-NES
F
Fluorescence (a.u.)
15
10
5
0
Bik1
Bik1-NES

Figure 2

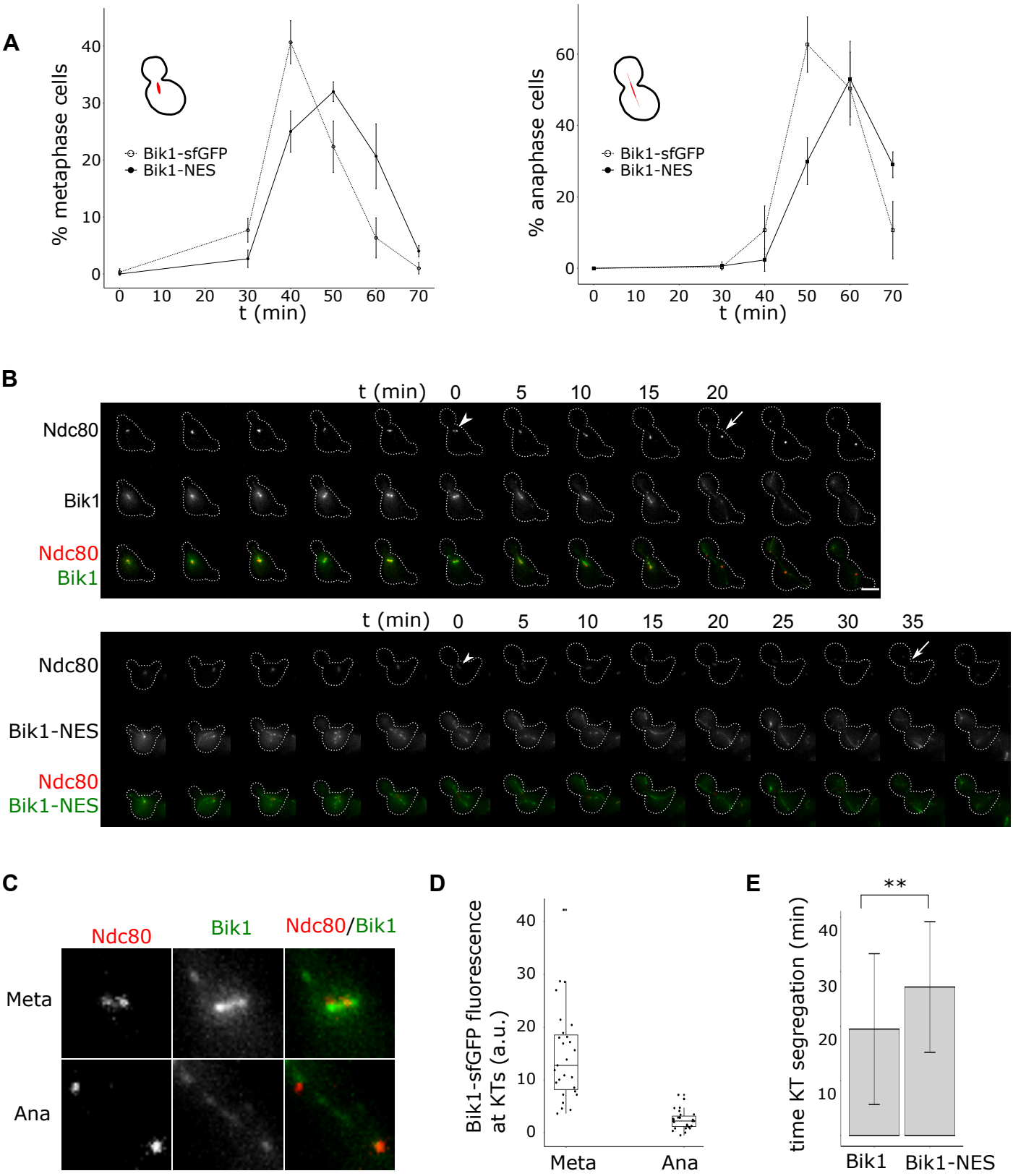
A
% metaphase cells
Bik1-sfGFP
Bik1-NES
t (min)
% anaphase cells
Bik1-sfGFP
Bik1-NES
t (min)
B
t (min) 0 5 10 15 20
Ndc80
Bik1
Ndc80
Bik1
t (min) 0 5 10 15 20 25 30 35
Ndc80
Bik1-NES
Ndc80
Bik1-NES
C
Ndc80
Bik1
Ndc80/Bik1
Meta
Ana
D
Bik1-sfGFP fluorescence at KTs (a.u.)
Meta
Ana
E
**
time KT segregation (min)
Bik1
Bik1-NES

Figure 3

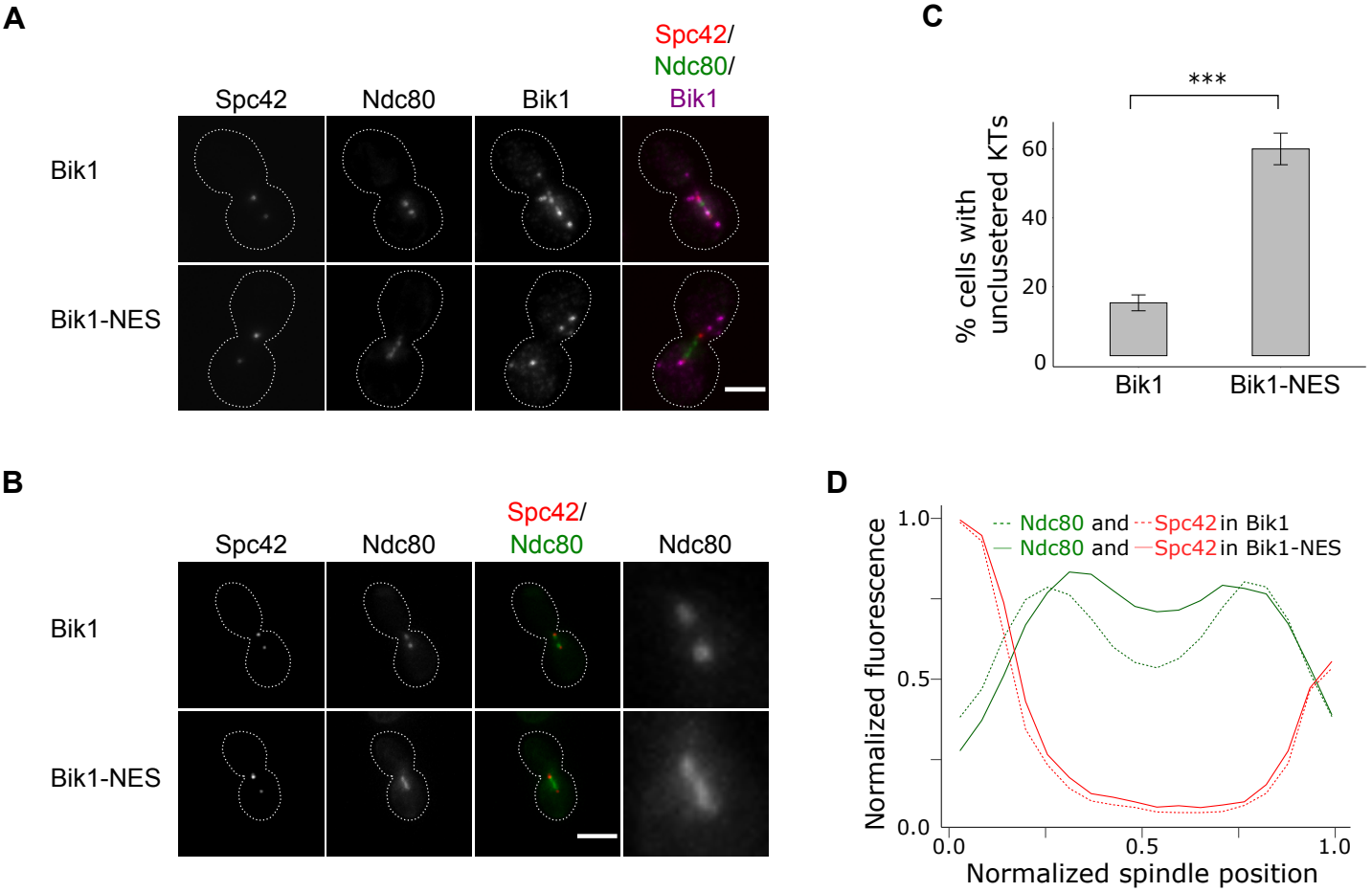
A
Spc42
Ndc80
Bik1
Spc42/
Ndc80/
Bik1
Bik1
Bik1-NES
B
Spc42
Ndc80
Spc42/
Ndc80
Ndc80
Bik1
Bik1-NES
C
***
% cells with unclusetered KTs
0
20
40
60
Bik1
Bik1-NES
D
Ndc80 and Spc42 in Bik1
Ndc80 and Spc42 in Bik1-NES
Normalized fluorescence
0.0
0.5
1.0
Normalized spindle position

Figure 4

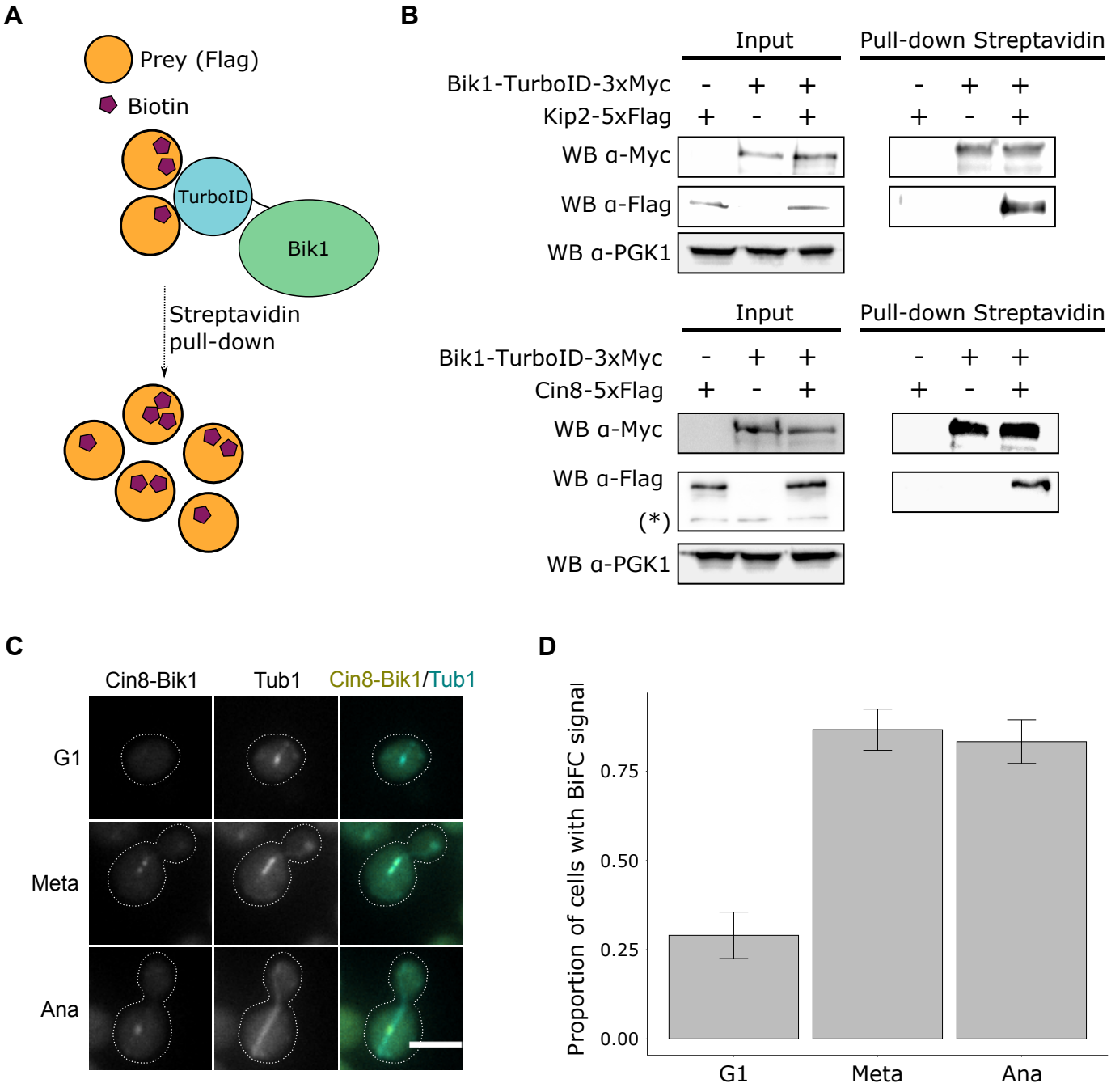
A
Prey (Flag)
Biotin
TurboID
Bik1
Streptavidin
pull-down
B
Input
Pull-down Streptavidin
Bik1-TurboID-3xMyc
Kip2-5xFlag
WB α-Myc
WB α-Flag
WB α-PGK1
Input
Pull-down Streptavidin
Bik1-TurboID-3xMyc
Cin8-5xFlag
WB α-Myc
WB α-Flag
(*)
WB α-PGK1
C
Cin8-Bik1
Tub1
Cin8-Bik1/Tub1
G1
Meta
Ana
D
Proportion of cells with BiFC signal
0.00
0.25
0.50
0.75
G1
Meta
Ana

Figure 5

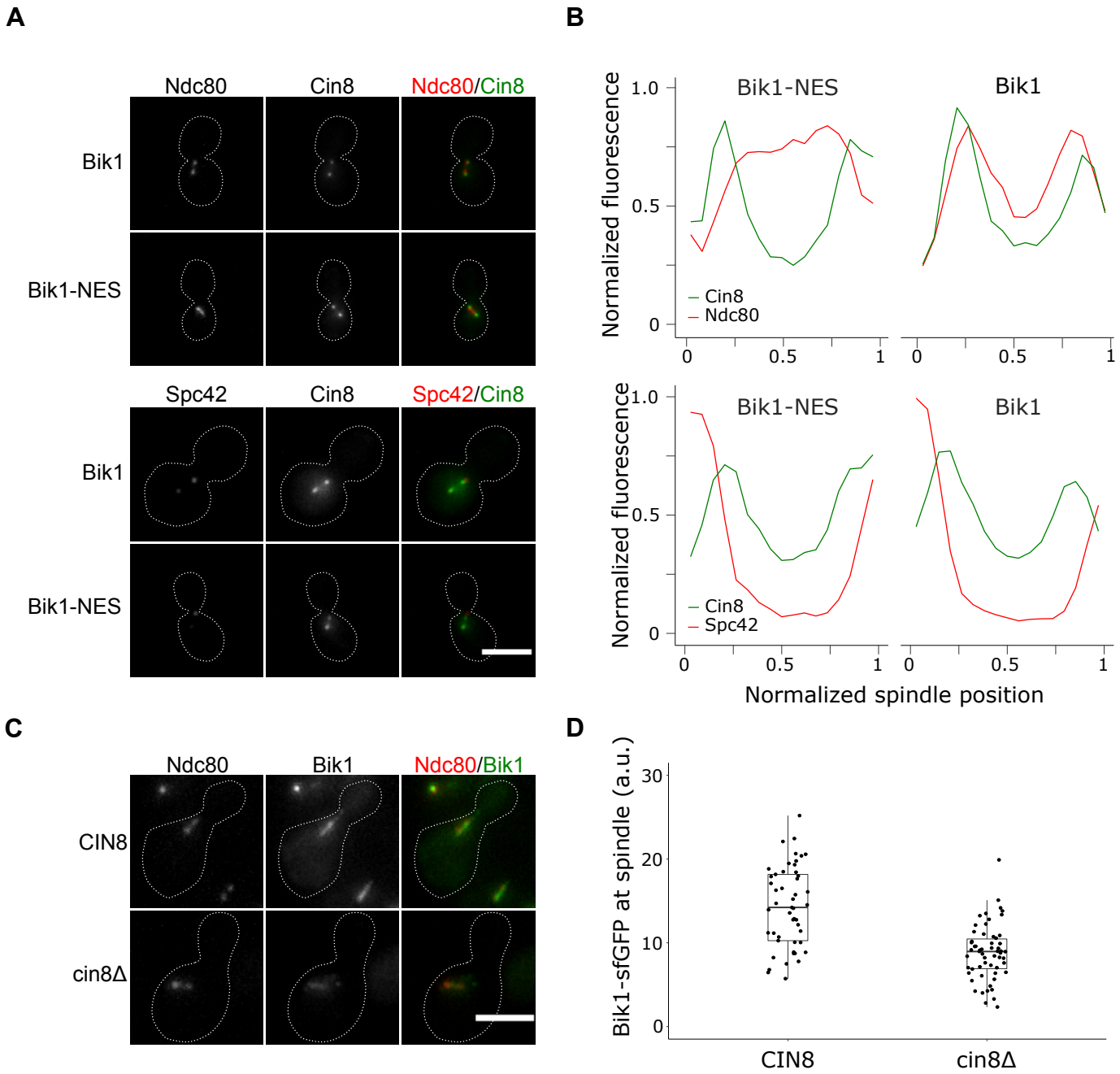
A
Ndc80
Cin8
Ndc80/Cin8
Bik1
Bik1-NES
Spc42
Cin8
Spc42/Cin8
Bik1
Bik1-NES
B
Bik1-NES
Bik1
Normalized fluorescence
1.0
0.5
0
Cin8
Ndc80
Cin8
Spc42
0
0.5
1
Normalized spindle position
C
Ndc80
Bik1
Ndc80/Bik1
CIN8
cin8Δ
D
Bik1-sfGFP at spindle (a.u.)
30
20
10
0
CIN8
cin8Δ

Table 1. A subset of the protein interactors of Bik1-FLAG (See Data S1 for a complete list).

Name	% Coverage	Unique peptides
STU2	72.33	104
BIM1	67.00	21
CIN8	50.67	46
KIP2	49.33	28
KAR9	47.33	26
KIP1	38.67	28
KAR3	38.67	23
CIK1	22.67	10
VIK1	21.00	10
KIP3	15.33	6

Table S1. Strains used in this study. All strains are derived from BY4741

Strain	Genotype
VMB-212	MATα BIK1-sfGFP:Ura3 SPC42-tagRFP-T:KanMX Leu2:HIS3p:mTurquoise2-TUB1
VMB-154	MATα BIK1-sfGFP:Ura3 NDC80-tagRFP-T:KanMX Leu2:HIS3p:mTurquoise2-TUB1
VMB-185	MATa BIK1-sfGFP:Ura3 NDC80-tagRFP-T:KanMX
VMB-293	MATa NatN2:PGAL1-CDC20 BIK1-sfGFP:Ura3 NDC80-tagRFP-T:KanMX
VMB-156	MATα BIK1-sfGFP-NES:NatMX NDC80-tagRFP-T:KanMX Leu2:HIS3p:mTurquoise2-TUB1
VMB-166	MATa BIK1-sfGFP:Ura3 Leu2:HIS3p:mRuby2-TUB1
VMB-209	MATa BIK1-sfGFP-NES:NatMX Leu2:HIS3p:mRuby2-TUB1
VMB-455	MATa HygroMX:PGAL1-CDC20 BIK1-5xFlag-NES:NatMX NDC80-sfGFP:Ura3 SPC42-tagRFP-T:KanMX
VMB-458	MATa HygroMX:PGAL1-CDC20 BIK1-5xFlag:NatMX NDC80-sfGFP:Ura3 SPC42-tagRFP-T:KanMX
VMB-433	MATa KIP2-5xFlag:KanMX
VMB-422	MATa BIK1-TurboID-3xMyc:NatMX
VMB-431	MATa BIK1-TurboID-3xMyc:NatMX KIP2-5xFlag:KanMX
VMB-393	MATa CIN8-5xFlag:KanMX
VMB-428	MATa BIK1-TurboID-3xMyc:NatMX CIN8-5xFlag:KanMX
VMB-448	MATa HygroMX:PGAL1-CDC20 CIN8-sfGFP:Ura3 NDC80-tagRFP-T:KanMX
VMB-453	MATa HygroMX:PGAL1-CDC20 BIK1-5xFlag-NES:NatMX CIN8-sfGFP:Ura3 NDC80-tagRFP-T:KanMX
VMB-459	MATa HygroMX:PGAL1-CDC20 BIK1-5xFlag:NatMX CIN8-sfGFP:Ura3 SPC42-tagRFP-T:KanMX
VMB-457	MATa HygroMX:PGAL1-CDC20 BIK1-5xFlag-NES:NatMX CIN8-sfGFP:Ura3 SPC42-tagRFP-T:KanMX
VMB-308	MATa BIK1-sfGFP:Ura3 cin8Δ:natMX NDC80-tagRFP-T:KanMX
VMB-288	MATa NatN2:PGAL1-CDC20 BIK1-5xFlag:KanMX
VMB-494	MATa BIK1-VN173:His3MX CIN8-VC155:KanMX Leu2:HIS3p:mTurquoise2-TUB1

Table S2. Plasmids used in this study

Plasmid	Relevant insert	Source
p44873	pFA6a-link-yosuperfolderGFP-CaURA3	Gift from Wendell Lim & Kurt Thorn (Addgene: 44873) PMID: 23844123
p44906	pFA6a-link-yoTagRFP-T-Kan	Gift from Wendell Lim & Kurt Thorn (Addgene: 44906) PMID: 23844123
p50641	pHIS3p:mTurquoise2-Tub1+3'UTR::LEU2	Gift from Wei-Lih Lee (Addgene: 50641) PMID: 25711127
p50645	pHIS3p:mRuby2-Tub1+3'UTR::LEU2	Gift from Wei-Lih Lee (Addgene: 50645) PMID: 25711127
pYM-N23	ScGAL1 promoter::pAgTEF-nat-tScADH1	PCR-Toolbox Knop (Euroscarf) MID: 15334558
p15983	pFA6a-5xFlag-KanMX6	Gift from Eishi Noguchi (Addgene: 15983) PMID: 18729046
	pFA6a-5xFlag-NatMX6	This study (subclonned from p15983)
pFB1434	pFA6a-Turbo-ID-3Myc-NatMX6	Gift from François Bachand (Addgene: 126050) PMID: 31064814
P30555	pFA6a-VN-His3MX6	Gift from Sung MK & Huh WK. (Euroscarf) PMID: 17534848
P30560	pFA6a-VC-kanMX6	Gift from Sung MK & Huh WK. (Euroscarf) PMID: 17534848